Supporting Information for Journal of Materials Chemistry A

Physically entangled multifunctional eutectogels for flexible sensors with mechanically robust

*Qianwen Lu,[a] Hengfeng Li [*a] and Zhijian Tan [*b]*

[a] *School of Materials Science and Engineering, Central South University, Changsha 410083, Hunan P. R. China.*

[b] *Institute of Bast Fiber Crops, Chinese Academy of Agricultural Sciences, Changsha 410205, Hunan, P. R. China.*

*To whom correspondence should be addressed.

E-mail: lihf@csu.edu.cn (H. Li); tanzhijian@caas.cn (Z. Tan)

Table of contents

1. Definitions of abbreviations

AA: acrylic acid; PAA: poly(acrylic acid); ChCl: choline chloride; Ca: catechol; CC: ChCl−Ca; Re: resorcinol; CR: ChCl−Re; Hy: hydroquinone; CH: ChCl−Hy; EA: ethyl acetate; PEGDA: poly(ethylene glycol) diacrylate; Irgacure 1173: 2-hydroxy-2-methylpropiophenone; CS: cefotaxime sodium; PU: polyurethane; PMMA: poly(methyl methacrylate), PTFE: polytetrafluoroethylene.

2. Comparison of eutectogels as sensors

Table S1. Comparison of eutectogels as strain sensors

Overview		Tensile strength (MPa)	Elongation (%)	Adhesion	Self-healing	Temperature adaptability	Antibacterial activity
2021[1]	Supramolecular-polymer double-network eutectogels	0.26	4400	✓	✓	✓	✗
2022[2]	PVI-based eutectogels	0.49	2300	✓	✓	✓	✗
2022[3]	WPU-based eutectogels	6.09	1707	✓	✗	✗	✗
2023[4]	Hydrophilic/hydrophobic heterostructure eutectogels	0.06	330	✗	✗	✓	✓
2023[5]	Supramolecular-polymer double-network eutectogels	0.21	4300	✓	✓	✓	✗
2022[6]	Cellulose-based eutectogels	1.25	1400	✓	✓	✓	✗
2023[7]	Polymeric eutectogels	8.8	1100	✓	✓	✓	✗
2021[8]	Binary polymer-based eutectogels	2.6	6.8	✗	✓	✗	✗
2022[9]	PVA-based eutectogels	20.2	550	✓	✓	✗	✗
2023[10]	SR-PVA eutectogels	1.67	590	✗	✗	✓	✗
2021[11]	WPU-based eutectogels	1.12	178	✓	✗	✗	✗
2023[12]	Dual crosslinked eutectogels	6.17	1067	✗	✓	✓	✗
2023[13]	Lignin-based eutectogels	0.05	460	✓	✗	✓	✗
2023[14]	Hydrophobic eutectogels	0.25	400	✓	✓	✗	✗
2023[15]	Double-network binary solvent eutectogels	3.25	574	✗	✗	✓	✓
2023[16]	PU-based eutectogels	4.1	1110	✗	✓	✓	✓
This work	PAA/CC eutectogels	8.04	620.5	✓	✓	✓	✓

3. Experimental section

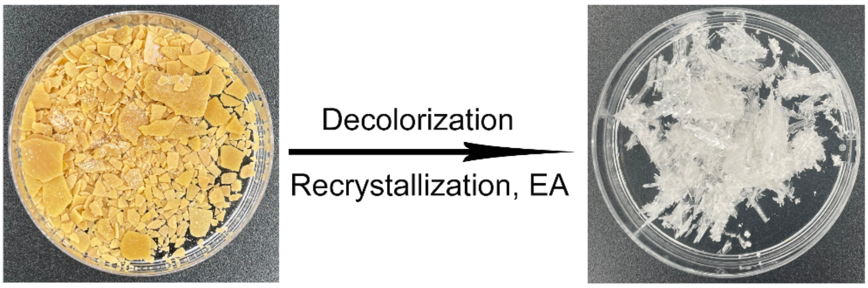

Figure S1. The decolorization and recrystallization of Ca.

Table S2. Six types of DESs.

DESs	HBA (g)	HBD (g)	Molar ratios
ChCl-Ca-1 (CC-1)	27.9	22.0	1:1
ChCl-Ca (CC)	27.9	44.0	1:2
ChCl-Re-1 (CR-1)	27.9	22.0	1:1
ChCl-Re (CR)	27.9	44.0	1:2
ChCl-Hy-1(CH-1)	27.9	22.0	1:1
ChCl-Hy (CH)	27.9	44.0	1:2

Table S3. PAA eutectogels with different kinds of DESs.

	AA (g)	DES (g)	1173 (mg)	PEGDA (mg)	Tensile fracture stress (MPa)	Tensile fracture strain (%)	Work of extension at fracture (MJ m^{-3})	Healing efficiency (%)	σ (S m^{-1})
PAA/CC$_{60}$-1	4	6	40	0	0.672	1528.2	4.07±1.13	92.15	1.42±0.06
PAA/CR$_{60}$-1	4	6	40	0	0.619	2309.2	5.34±0.67	83.53	1.14±0.12
PAA/CH$_{60}$-1	4	6	40	0	0.525	2465.9	7.65±0.49	79.91	0.93±0.08
PAA/CC	4	6	40	0	8.044	620.5	28.69±2.23	72.71	0.43±0.07
PAA/CR$_{60}$	4	6	40	0	5.336	653.7	16.92±1.14	77.14	0.82±0.04
PAA/CH$_{60}$	4	6	40	0	4.656	792.5	26.97±2.31	74.11	0.77±0.06

Table S4. PAA eutectogels with different CC and PEGDA contents.

	AA (g)	DES (g)	1173 (mg)	PEGDA (mg)	Tensile fracture stress	Tensile fracture strain	Work of extension at fracture	Healing efficiency (%)	σ (S m^{-1})

					(MPa)	(%)	(MJ m^{-3})		
PAA/CC$_{50}$	5	5	50	0	18.136	525.5	60.96±1.33	50.70	0.25±0.01
PAA/CC	4	6	40	0	8.044	620.5	28.69±2.23	72.71	0.43±0.07
PAA/CC$_{60}$P$_{0.1}$	4	6	40	22.2	5.377	575.2	18.40±2.09	68.84	0.53±0.06
PAA/CC$_{60}$P$_{0.25}$	4	6	40	55.5	4.520	487.9	11.32±1.37	65.10	0.69±0.02
PAA/CC$_{60}$P$_{0.5}$	4	6	40	111.0	4.481	413.7	10.48±0.41	59.23	0.72±0.06
PAA/CC$_{60}$P$_{0.75}$	4	6	40	166.5	3.936	365.2	7.36±1.56	55.35	0.91±0.01
PAA/CC$_{60}$P$_{1.0}$	4	6	40	222.0	3.628	296.9	7.47±1.40	53.83	0.85±0.03
PAA/CC$_{70}$	3	7	30	0	1.220	1149.0	6.36±1.32	86.00	0.68±0.04

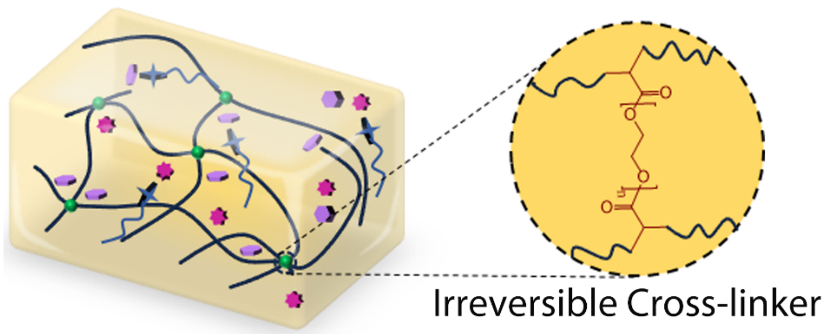

Figure S2. Schematic fabrication diagram of PAA/CC eutectogel, when polymerizing with the presence of PEGDA.

4. Simulation calculation of the PAA/CC eutectogel

Interaction energy: The symmetry-adapted perturbation theory (SAPT) interaction energy was calculated using P_{SI}4 software under the level of sSAPT/jun-cc-pVTZ standard and the independent gradient model based on the Hirshfeld partition (IGMH) method in multiwfn.[17-19] The polymer chain was simplified into ten repeated AA components.

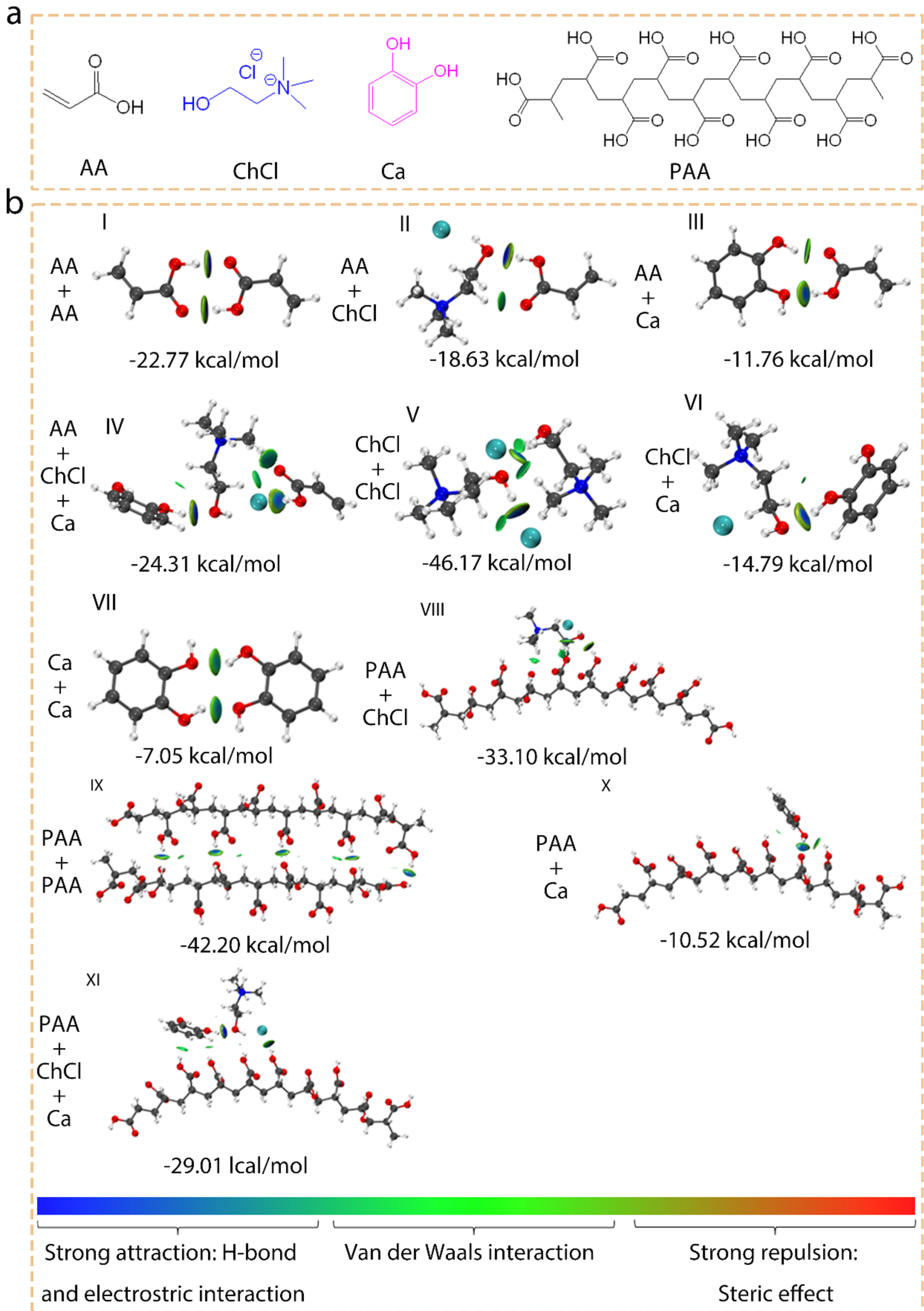

Figure S3. Chemical structures and SAPT analysis of AA, ChCl, Ca, and PAA: (a) Chemical structures of AA, ChCl, Ca, and PAA; (b) Different combination modes and the IGM isosurfaces between AA, ChCl, Ca, and PAA.

Table S5. Results of the SAPT analysis for interaction energy between AA, PAA, ChCl, and Ca.

Combination modes	$E_{electrostatics}$ (kcal mol^{-1})	$E_{exchange}$ (kcal mol^{-1})	$E_{introduction}$ (kcal mol^{-1})	$E_{dispersion}$ (kcal mol^{-1})	E_{total} (kcal mol^{-1})
I	-34.92	35.15	-16.60	-6.40	-22.77
II	-25.30	21.60	-9.39	-5.55	-18.63
III	-20.06	21.34	-7.80	-5.24	-11.76
IV	-31.69	26.86	-12.42	-7.06	-24.31
V	-59.16	44.75	-18.92	-12.85	-46.17
VI	-20.14	18.53	-7.03	-6.15	-14.79
VII	-12.97	13.28	-2.94	-4.42	-7.05
VIII	-40.81	33.82	-13.78	-12.33	-33.10
IX	-62.74	59.14	-25.21	-13.58	-42.40
X	-20.25	24.17	-8.19	-6.25	-10.52
XI	-32.21	30.67	-11.21	-17.26	-29.01

Cohesive energy density (*CED*): Three simplified molecular models of PAA/CC were built. The cohesive energy density (CED) was carried out using the Materials Studio (MS) software package[20] shown in Figure 1c and Figure S2. It was calculated according to Eqs. 1-2.

$$CED = \frac{E_{coh}}{V} \qquad (1)$$

$$E_{coh} = E_{intra} - E_{total} \qquad (2)$$

where E_{coh} is the cohesive energy, V is the volume of a system, E_{intra} is the intramolecular electrostatic energy, and E_{total} is the total electrostatic energy of a system.[21, 22]

The calculation details were the same as in our previous work.[23]

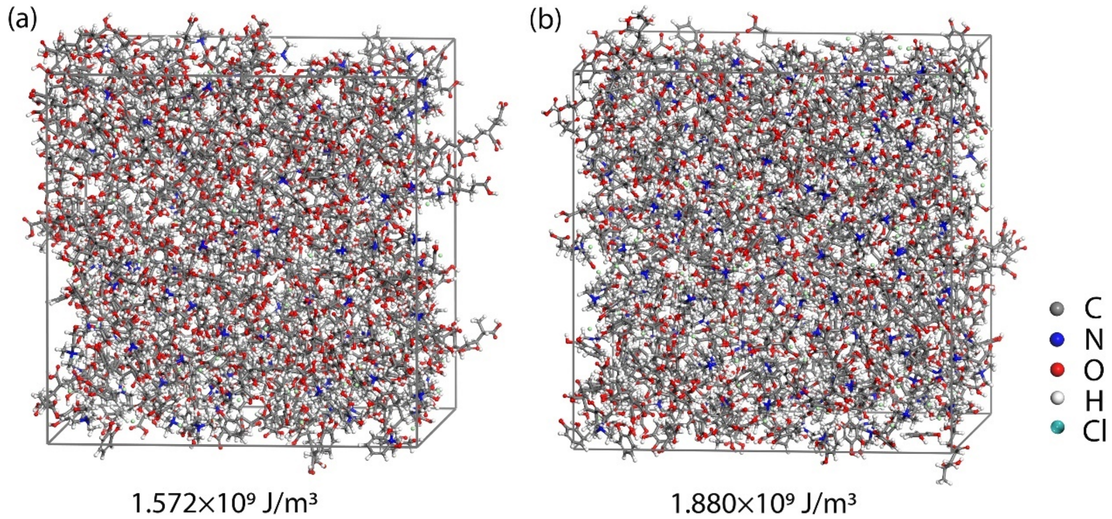

Figure S4. CED molecular models of PAA/CC: (a) The content of CC is 50 wt% (60 PAA molecules; 120 ChCl molecules; 240 Ca molecules); (b) The content of CC is 70 wt% (36 PAA molecules; 181 ChCl molecules; 362 Ca molecules).

5. Characterization of the PAA/CC eutectogel

5.1 Fourier transform infrared (FTIR) and ^1H nuclear magnetic resonance (^1H NMR) spectra of PAA/CC

FTIR spectra were recorded by a Thermo Scientific Nicolet iS10 FTIR spectrometer from 4000 to 400 cm^{-1} at room temperature. ^1H NMR spectra were acquired by a Bruker-AVANCE III 500 spectrometer at room temperature with the use of the CD_3OD.

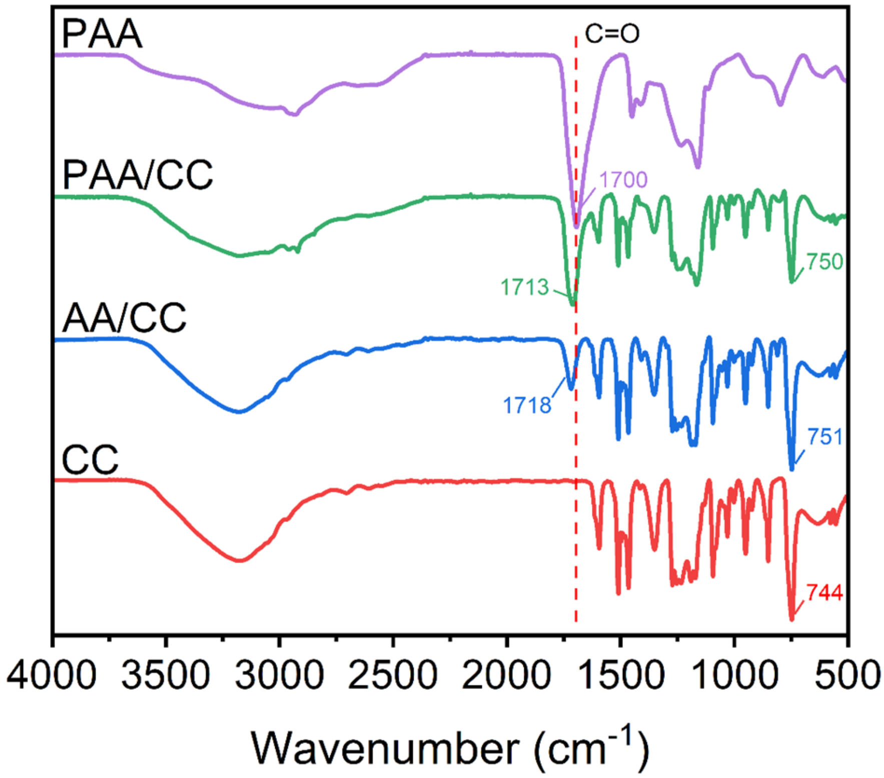

Figure S5. The FTIR spectra of PAA hydrogel, PAA/CC eutectogel, AA/CC, and CC.

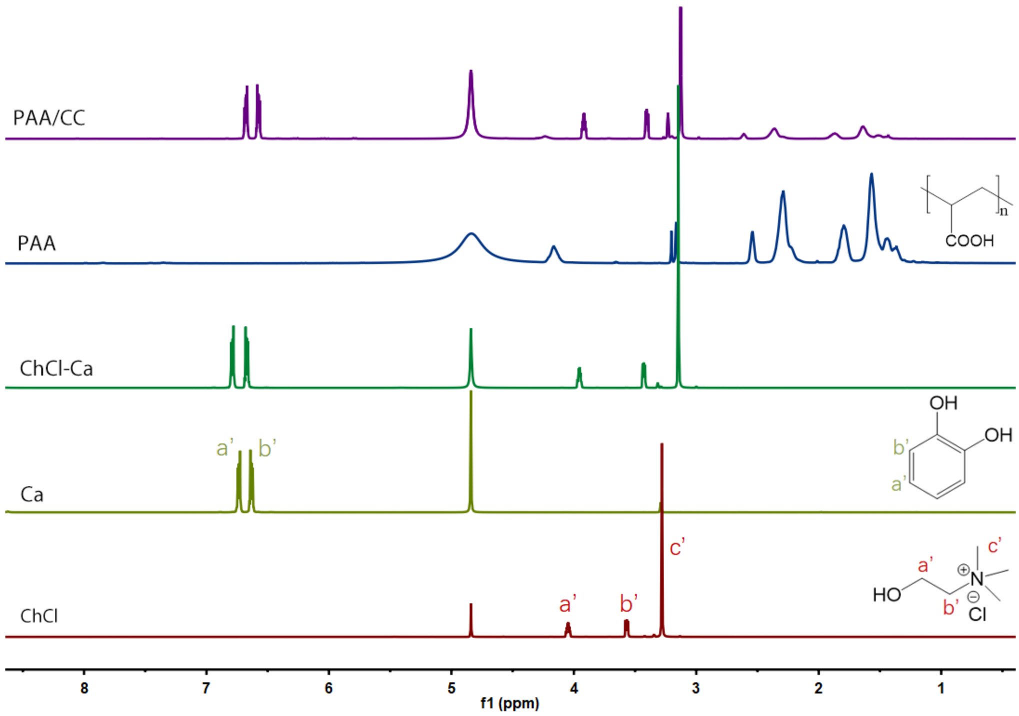

Figure S6. The ^{1}H NMR spectra (500 MHz, CD_3OD, room temperature) of ChCl, Ca, CC, PAA hydrogel and PAA/CC eutectogel.

5.2 The mechanical, adhesive, self-healing, and conductive performances of PAA/CC eutectogel

The transparency of PAA/CC eutectogel: The transparency test was performed in a transmittance tester (RK-6000T, Guangzhou Ruike Optoelectronic Technology Co., Ltd., China). A square eutectogel sheet (20 mm × 20 mm × 1 mm) was used.

Mechanical performance of PAA/CC eutectogel: The tensile and cyclic stretch-release tests were conducted in materials universal testing machine with a 500 N load cell. The velocities of tensile and cyclic stretch-release are 200 and 500 mm min^{-1}, respectively. The compressive tests were conducted using a materials universal testing machine with a 5000 N load cell at a speed of 20 mm min^{-1}.

Rheological tests: The rheological tests were performed on an Anton Paar MCR 92 rheometer. The roto PP25 with a diameter of 25 mm was used and the gap at 1mm. The frequency sweep tests were conducted from 0.1 to 100 rad/s with 1% constant strain. The stepwise strain tests were carried out at a small strain of 0.1% and a big strain of 100%. The temperature sweep tests were executed from 25 to 110 ºC.

Thermogravimetric analysis (TGA) tests: The TGA data were collected by a Shimadzu TGA-50/50H at 10 ºC min^{-1} from 25 ºC to 800 ºC in a nitrogen atmosphere.

Differential scanning calorimetry (DSC) tests: The DSC measurements were performed using a NETZSCH DSC 200F3 at 10 ºC min^{-1} from –100 ºC to 100 ºC under flowing nitrogen.

Dynamic thermomechanical analysis (DMA) tests: The DMA data were obtained on a DMAQ800-Waters Technology (China) Limited using the shear model.

Adhesive performance of PAA/CC eutectogels: The adhesion tests were conducted using the lap shear method[24] with the universal testing machine at 200 mm min^{-1}. All samples were sandwiched in between different pristine substrates, and two binder clips were placed on the specimens for 2 h to form intimate contact.

Low-temperature and high-temperature adhesion test: All specimens were stored at −20 or 80 ºC for 2 h before the adhesion tests.

Self-healing performance of PAA/CC eutectogels: To evaluate the self-healing ability of PAA/CC eutectogel, a rectangular eutectogel sheet (40 mm × 10 mm × 2 mm) was cut into two pieces. The two separated specimens were placed in contact at room temperature and dry environment for 12 h. Healing efficiency (HE) was defined as Eq. 3.

$$HE = \frac{BE_{Virgin}}{BE_{Healed}} \quad (3)$$

where BE_{Virgin} and BE_{Healed} are breaking elongations of virgin and healed eutectogels.

Ionic conductivity measurement: The measurement method was the same as in our previous work.[23] Briefly, the ionic conductivity of eutectogels was measured by a three-probe method via an electrochemical workstation (DH7000C). Three conductive data were recorded for each sample. The ionic conductivity (σ) was calculated by Eq. 4.

$$\sigma = \frac{L}{RS} \quad (4)$$

where R is the resistance, S is the surface area of the measured eutectogels, and L is the thickness of the measured eutectogels.

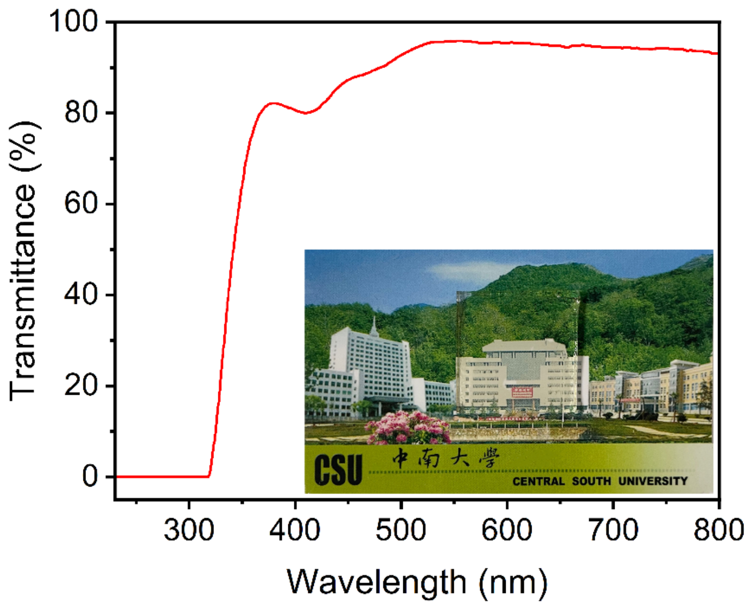

Figure S7. Transmittance of PAA/CC. The inset image showed the excellent transparency of PAA/CC with a 1.0 mm thickness.

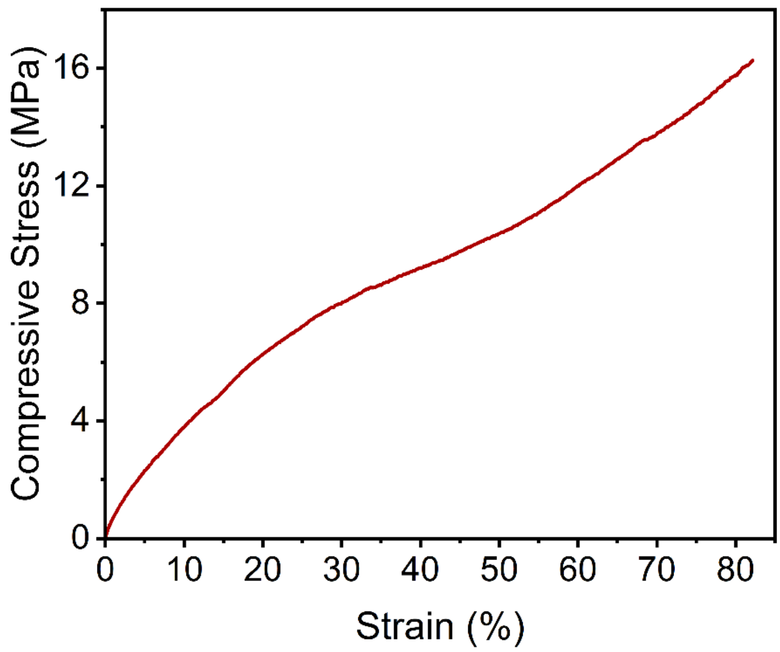

Figure S8. The compressive strain-stree cvure of PAA/CC.

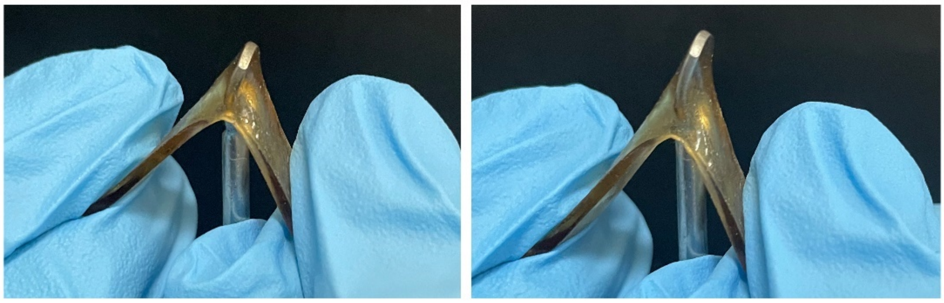

Figure S9. The photograph of PAA/CC blocks the piercing of blunt weapons.

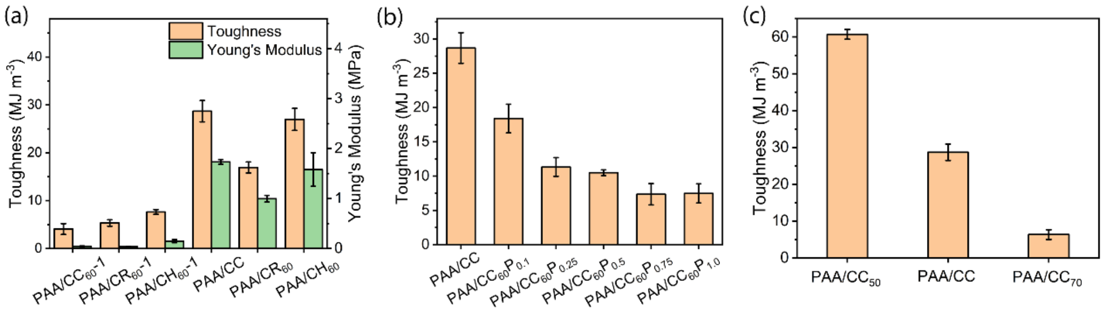

Figure S10. Toughness and Young's modulus values of: (a) The six eutectogels; (b) PAA/$CC_{60}P_y$ (y=0, 0.1, 0.25, 0.5, 0.75 and 1.0, mean the addition amount of crosslinking agent as 0.1%, 0.25%, 0.5%, 0.75% and 1.0% (mol/mol) of AA); (c) PAA/CC_x (x=50, 60, and 70, denote the CC content as 50%, 60%, and 70% (w/w)**).**

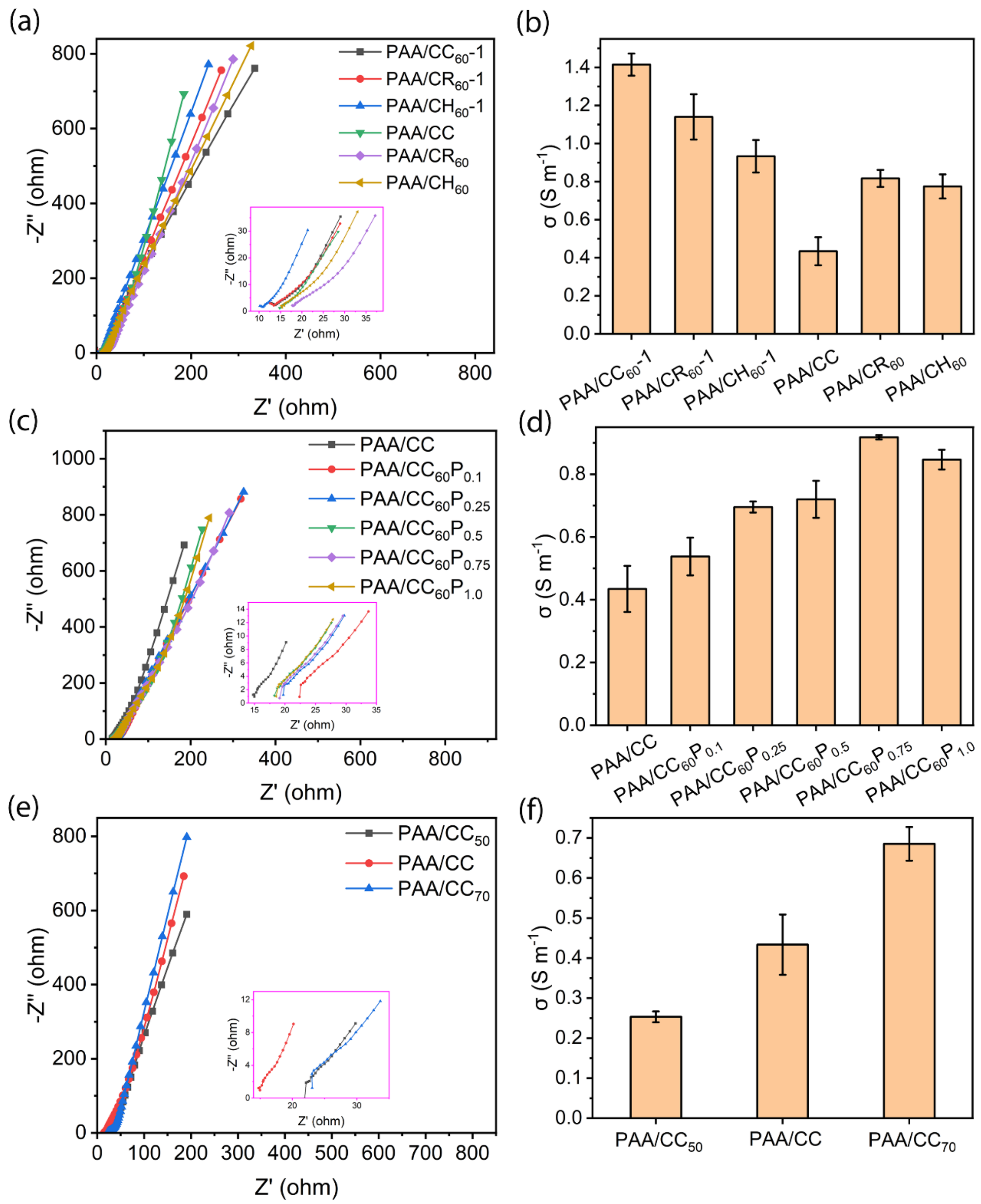

Figure S11. Ionic conductivity measurement: (a,b) Electrochemical impedance spectroscopy (EIS) and ionic conductivity of the six eutectogels; (c,d) EIS and ionic conductivity of PAA/$CC_{60}P_y$ (y=0, 0.1, 0.25, 0.5, 0.75 and 1.0, mean the addition amount of crosslinking agent as 0.1%, 0.25%, 0.5%, 0.75% and 1.0% (mol/mol) of AA); (e,f) EIS and ionic conductivity of PAA/CC_x (x=50, 60 and 70, denote the CC content as 50%, 60%, and 70% (w/w)).

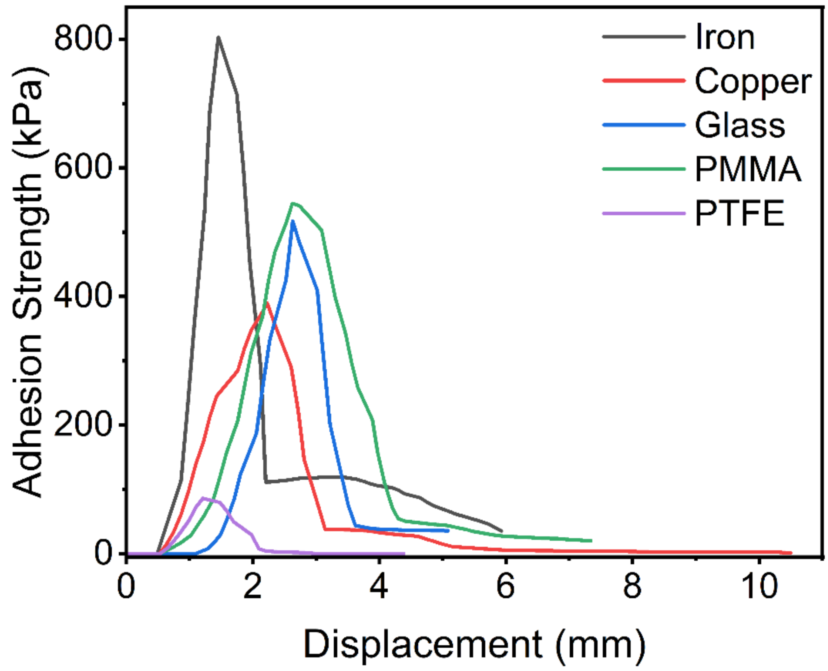

Figure S12. The adhesion lap-shear test of PAA/CC with different substrates (iron, copper, glass, PMMA, and PTFE).

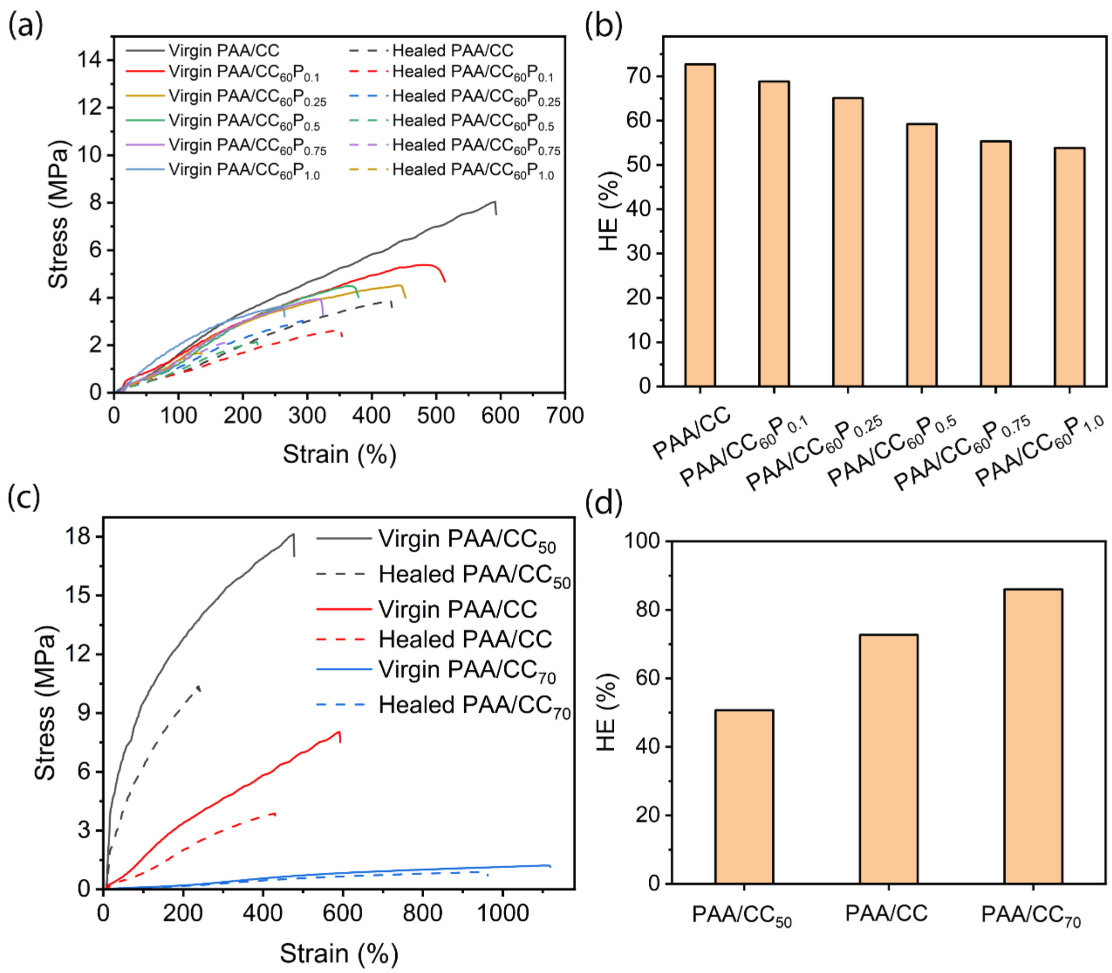

Figure S13. The tensile strain-stress curves and effectiveness of: (a,b) PAA/$CC_{60}P_y$ (y=0, 0.1, 0.25, 0.5, 0.75 and 1.0, mean the addition amount of crosslinking agent as 0.1%, 0.25%, 0.5%, 0.75% and 1.0% (mol/mol) of AA); (c,d) PAA/CC_x (x=50, 60, and 70, denote the CC content as 50%, 60%, and 70% (w/w)).

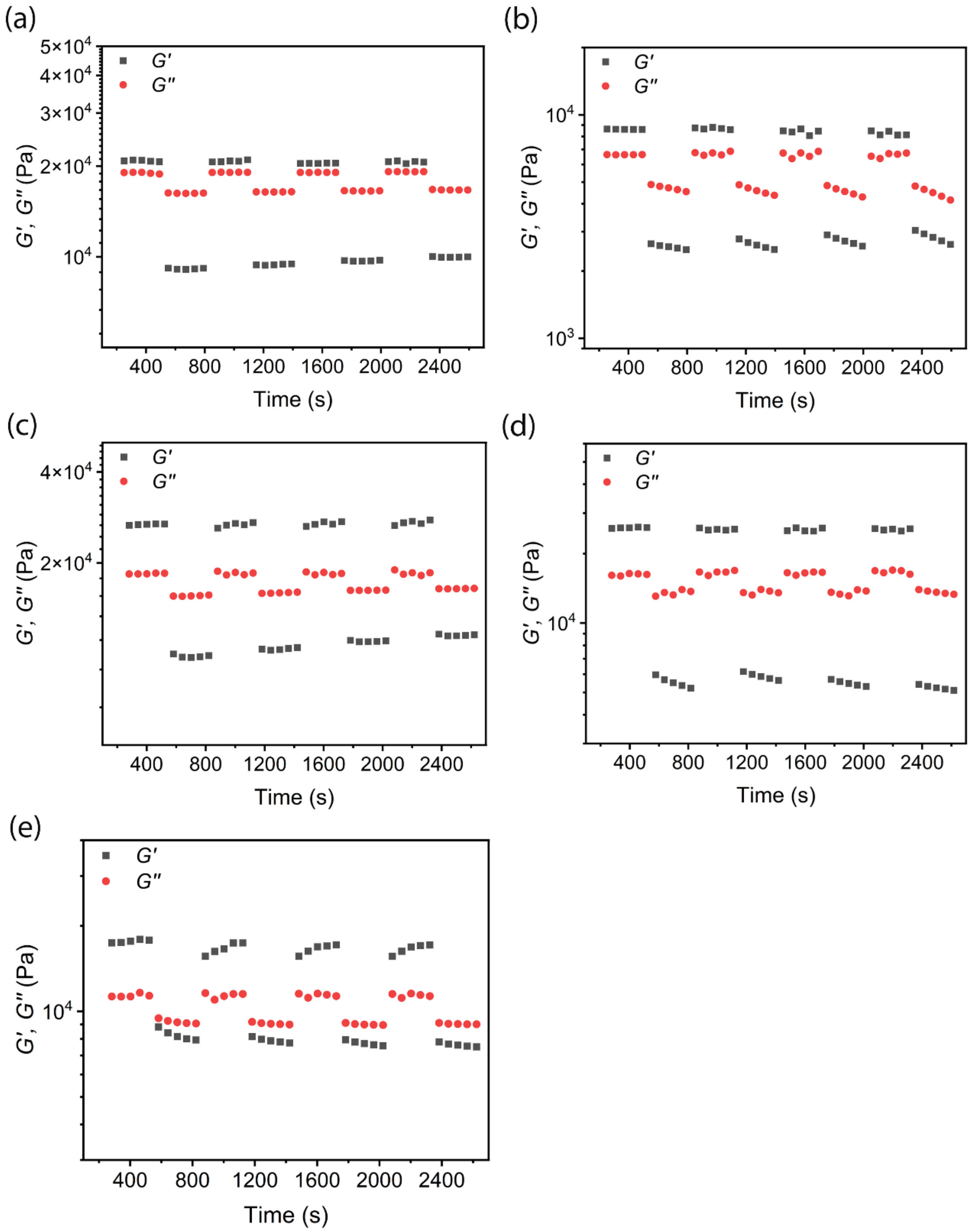

Figure S14. The rheological stepwise strain test of: (a) PAA/CC_{60}-1; (b) PAA/CH_{60}-1; (c) PAA/CR_{60}-1; (d) PAA/CH_{60}; (e) PAA/CR_{60}.

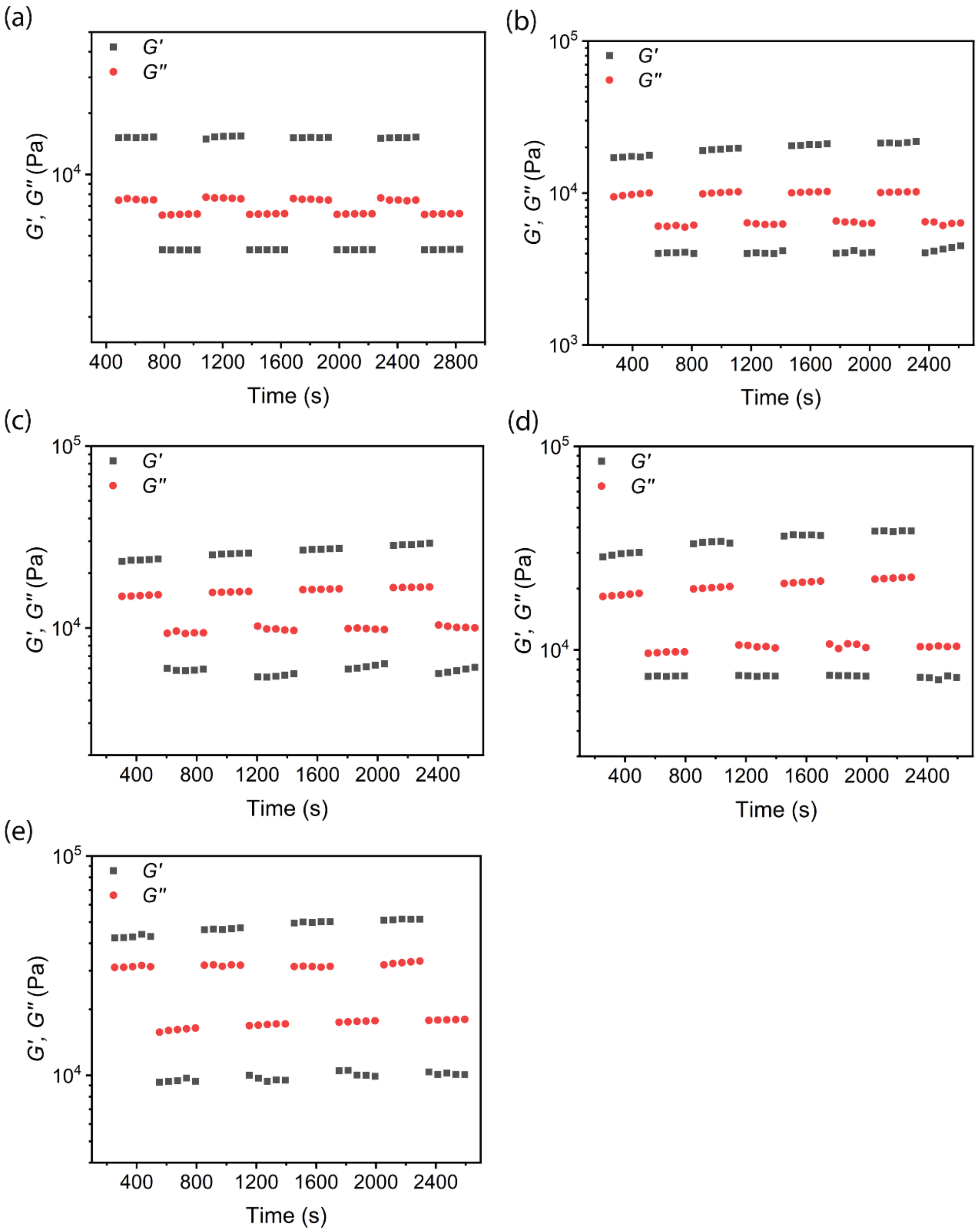

Figure S15. The rheological stepwise strain test of: (a) PAA/$CC_{60}P_{0.1}$; (b) PAA/$CC_{60}P_{0.25}$; (c) PAA/$CC_{60}P_{0.5}$; (d) PAA/$CC_{60}P_{0.75}$; (e) PAA/$CC_{60}P_{1.0}$.

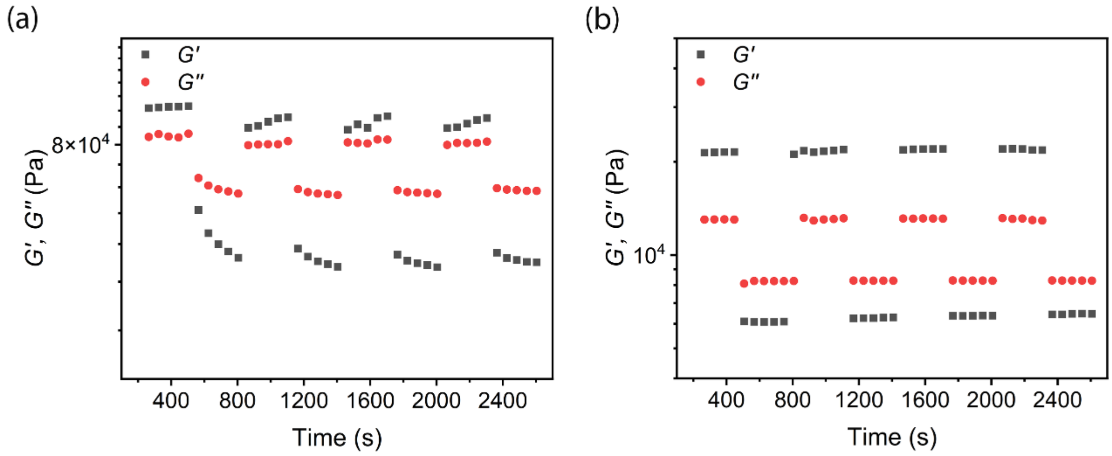

Figure S16. The rheological stepwise strain test of: (a) PAA/CC_{50}; (b) PAA/CC_{70}.

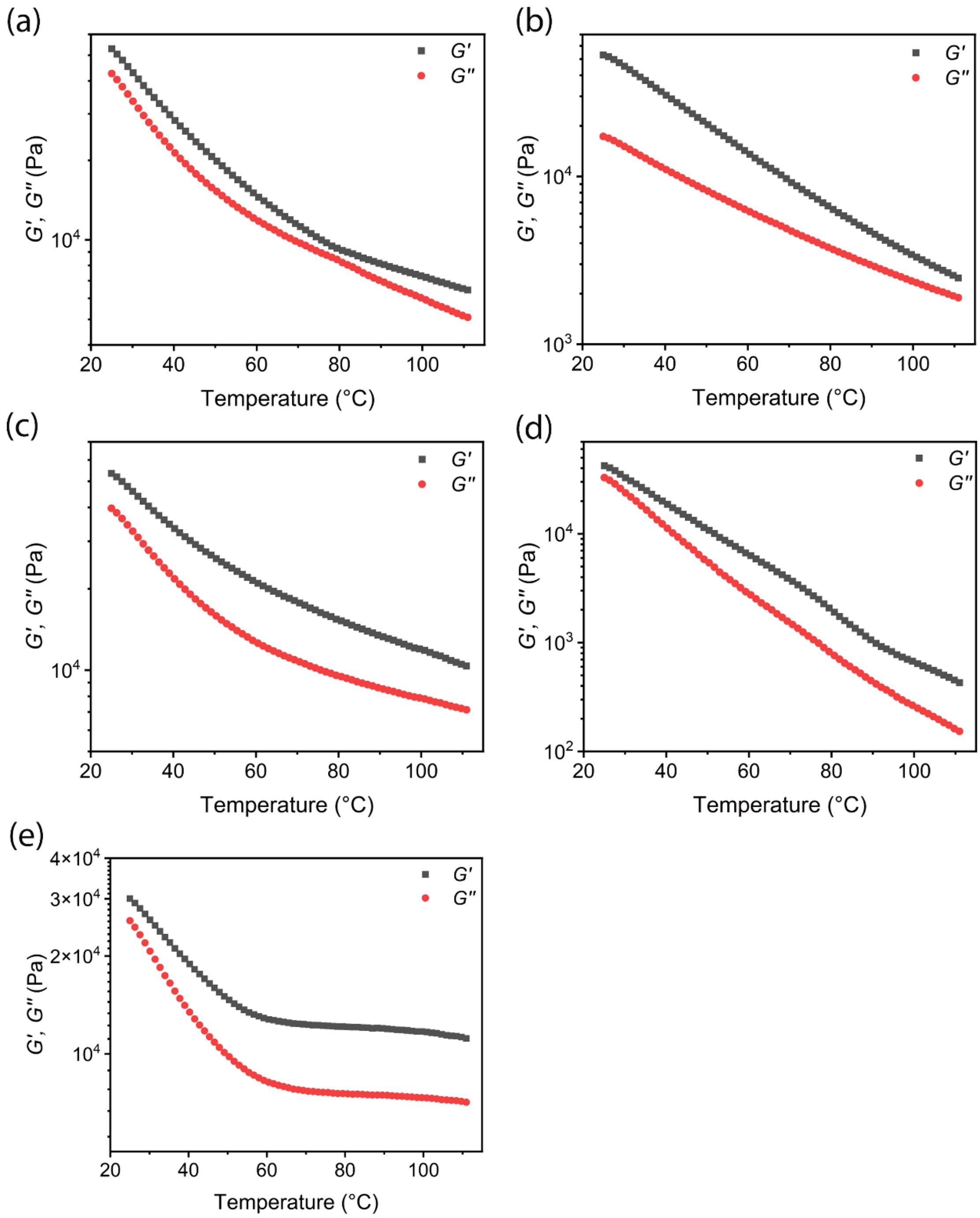

Figure S17. The temperature ramp rheological test with the temperature ranging from 25 ºC to 110 ºC. (a) PAA/CC_{60}-1. (b) PAA/CH_{60}-1. (c) PAA/CR_{60}-1. (d) PAA/CH_{60}. (e) PAA/CR_{60}.

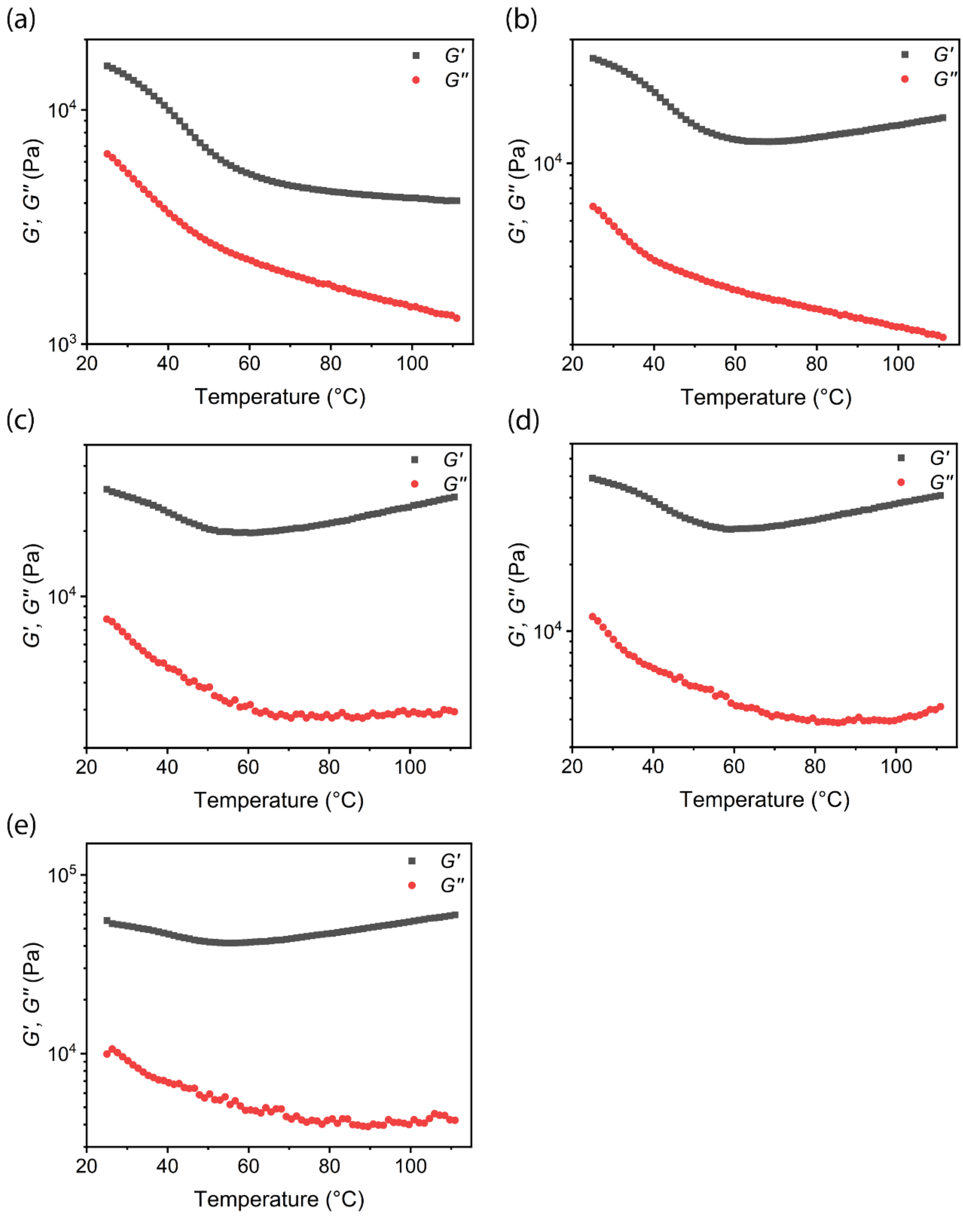

Figure S18. The temperature ramp rheological test with the temperature ranging from 25 ºC to 110 ºC. (a) PAA/$CC_{60}P_{0.1}$. (b) PAA/$CC_{60}P_{0.25}$. (c) PAA/$CC_{60}P_{0.5}$. (d) PAA/$CC_{60}P_{0.75}$. (e) PAA/$CC_{60}P_{1.0}$.

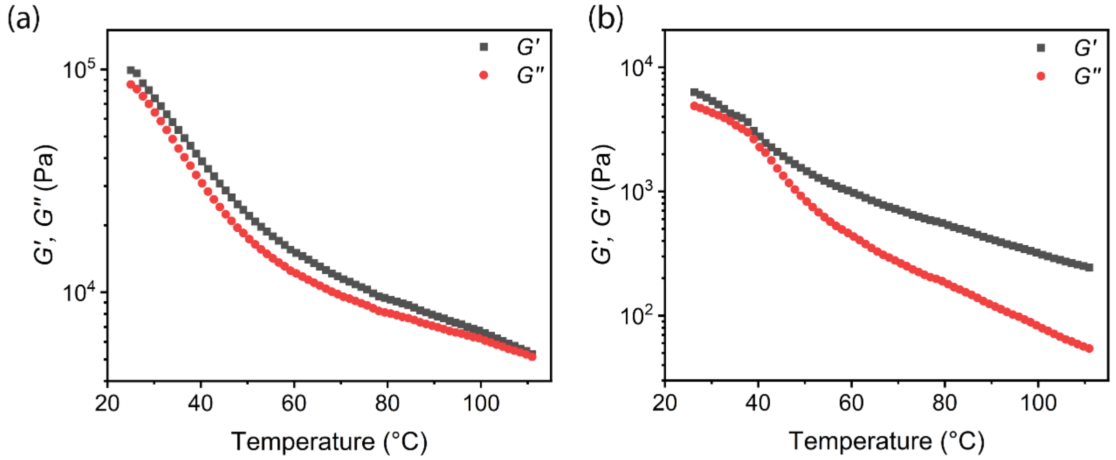

Figure S19. The temperature ramp rheological test with the temperature ranging from 25 ºC to 110 ºC. (a) PAA/CC_{50}. (b) PAA/CC_{70}.

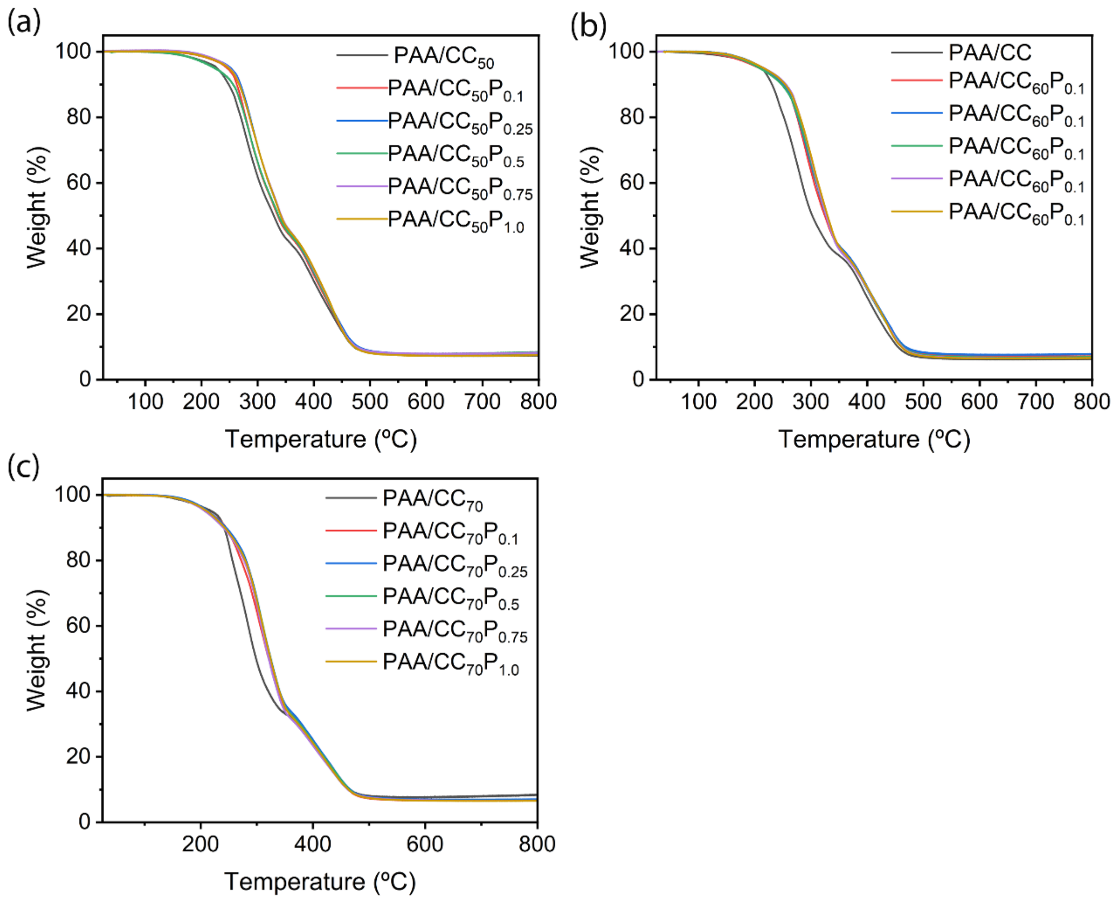

Figure S20. TGA spectra of: (a) PAA/$CC_{50}P_y$ (y=0, 0.1, 0.25, 0.5, 0.75 and 1.0, mean the addition amount of crosslinking agent as 0.1%, 0.25%, 0.5%, 0.75% and 1.0% (mol/mol) of AA); (b) PAA/$CC_{60}P_y$ (y=0, 0.1, 0.25, 0.5, 0.75 and 1.0, mean the addition amount of crosslinking agent as 0.1%, 0.25%, 0.5%, 0.75% and 1.0% (mol/mol) of AA); (c) PAA/$CC_{70}P_y$ (y=0, 0.1, 0.25, 0.5, 0.75

and 1.0, mean the addition amount of crosslinking agent as 0.1%, 0.25%, 0.5%, 0.75% and 1.0% (mol/mol) of AA).

Table S6. T_g of PAA hydrogel, PAA/CC eutectogel and CC DES.

Sample	T_g (°C)
PAA	48.59
CC	–
PAA/CC	−35.69

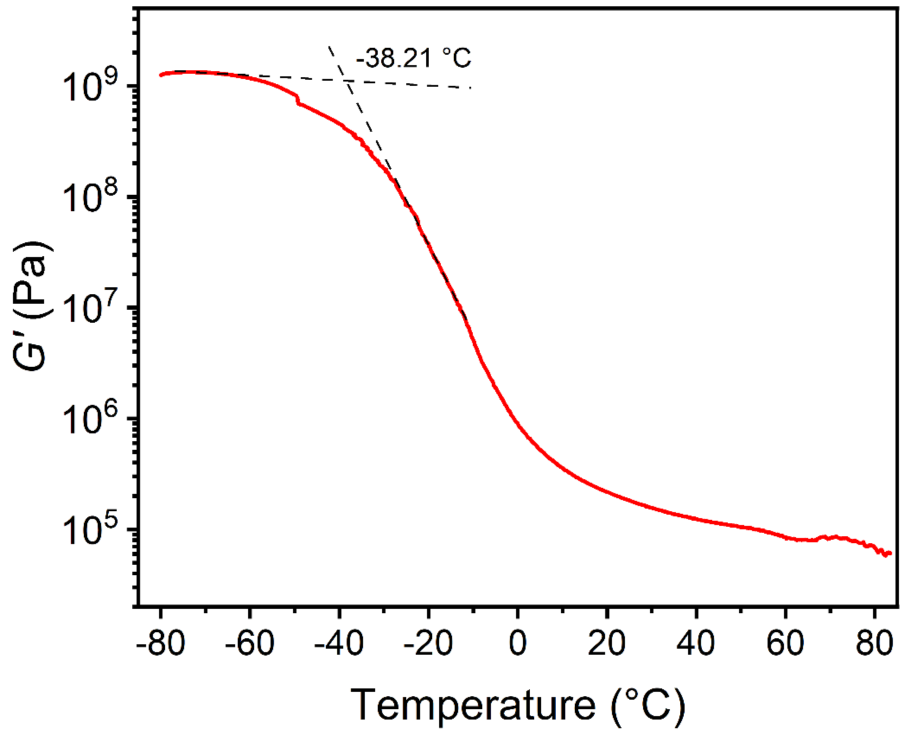

Figure S21. Temperature dependence of the storage modulus (*G'*) of PAA/CC.

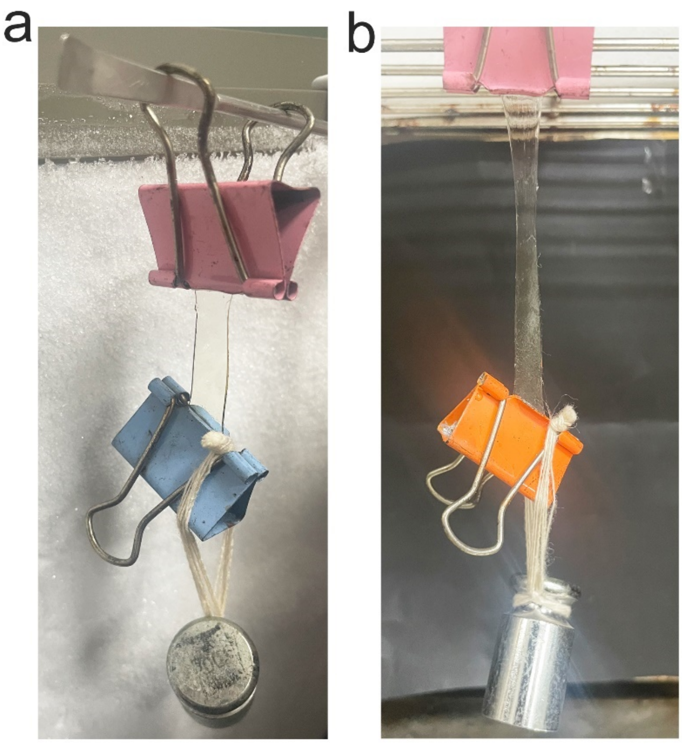

Figure S22. The photograph of temperature-tolerance of PAA/CC eutectogel. (a) Storing at -20 ºC for 24 h. (b) Storing at 80 ºC for 24 h.

5.3 The antibacterial performance of PAA/CC eutectogel

Antibacterial performance evaluation: The operation procedures are as follows:

Bacterial inhibition experiment: The antibacterial performance of eutectogel was evaluated against *Escherichia coli* (*E. coil*, Gram-negative bacteria) and *Staphylococcus aureus* (*S. aureus*, Gram-positive bacteria) using two methods.

(a) Spread plate method: Bacteria seeds were cultured in Luria−Bertani (LB) broth liquid medium at 37 ºC with 180 rpm for 24 h. Then, the cultivated seeds were diluted with sterile water to 40 times. 10 μL of diluted bacterial liquid was evenly applied onto PAA/CC gels and solid LB broth (control group). The incubation was carried out at 37 ºC for 24 hours.

(b) Inhibition zone test (includes four steps):

(1) Specimens: PAA/CC eutectogels were dissolved in sterile water to prepare different concentrations of eutectogel solutions, named E_x (x= 350 and 400; denote the concentrations of eutectogels as 350 and 400 mg/mL). PAA hydrogel also was

dissolved in sterile water, the concentration was 400 mg/mL. 500 ppm of CS as a positive control. Soak the sterilized filter papers (diameter is 6 mm) into the above three solutions to prepare the specimens. Sterilized medical PU films (diameter is 6 mm) as a negative control.

(2) Culture of bacterial: 6 mL of bacterial suspensions of *E. coil* and *S. aureus* (solvents were sterile water) were obtained by scraping the different strains after 24 hours of resuscitation by LB broth. Two suspensions were cultured for 18 h in an intelligent shaker.

(3) Preparation of bacterial culture medium: Dilute the above bacterial suspension by 20 times, and pour them into LB broth, then cast them into an empty culture medium plate.

(4) Antibacterial experiments: Put the above specimens in bacterial culture medium, then they all were cultured under the set environment, i.e. 37 ℃, normal humidity, and normal atmospheric pressure. After 24 hours, we observed and recorded the survival of the bacteria by antibacterial zone size.

Notably, all procedures were performed in a sterile environment.

The antibacterial ability was calculated using Eq. 5.[25]

$$D_{zh} = \frac{R_z}{R_h} \qquad (5)$$

where R_z is the radius of the bacteriostatic zone; R_h is the radius of the materials.

Fungal inhibition experiment:

Potato dextrose agar (PDA) media were used to culture two kinds of fungus, *Rhizoctonia solani Kuhn* (*R. solani*) and *Fusarium oxysporum* f. sp. *nelumbicola* (*F. oxysporum*). The inhibition efficiencies of E_{400} and sterilized medical PU films were detected. All PDA media were put in the set environment (25 ºC, normal humidity, and normal atmospheric pressure). After 7 days, we observed and recorded the survival of the fungus by antibacterial zone size.

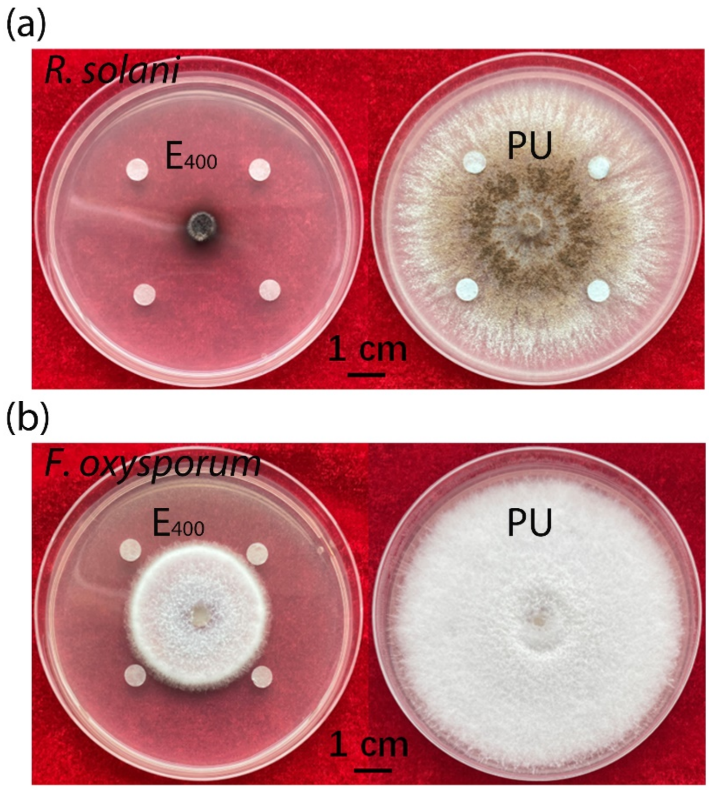

Figure S23. Antibacterial capability of PAA/CC to two types of fungus. (a) *R. solani*. (b) *F. oxysporum*.

6. Wearable strain sensor applications of PAA/CC eutectogel

A PAA/CC eutectogel sheet (30 mm × 10 mm × 1 mm) with copper plates connected at both ends was attached to the skin of a volunteer's joints. Connect the copper sheet to the test metal clamp. The real-time resistance response of the eutectogel under different strains was recorded by a sourcemeter Keithley 2450 at 2 V. Gauge factor (GF) is a significant index to access the sensitivity of eutectogel, which can be obtained by Eq. 6.

$$GF = \frac{(R - R_0)/R_0}{\varepsilon} \qquad (6)$$

where R_0 is the initial resistance of the eutectogel at rest, R is the real-time resistance during the stretching process and ε is imposed strain.

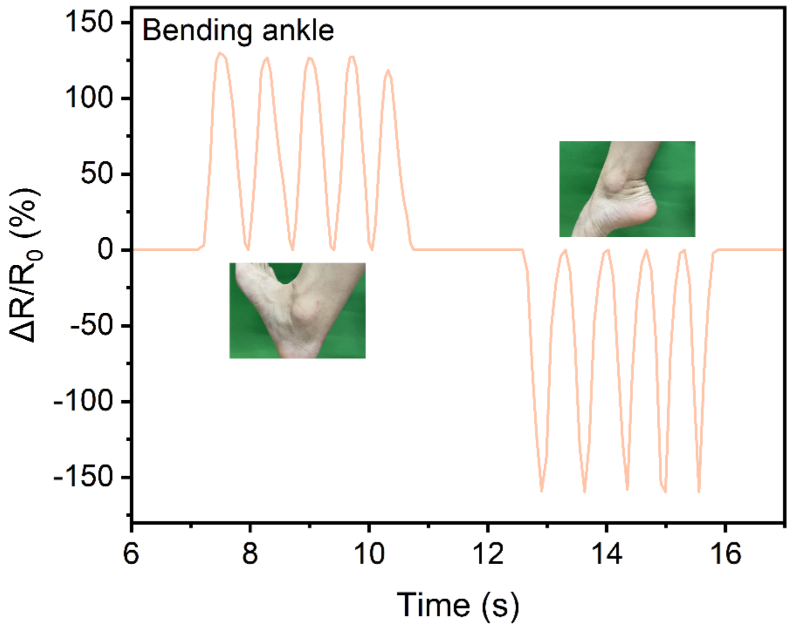

Figure S24. Continuous monitoring of ankle movements using the strain sensor across various movement directions and bending angles.

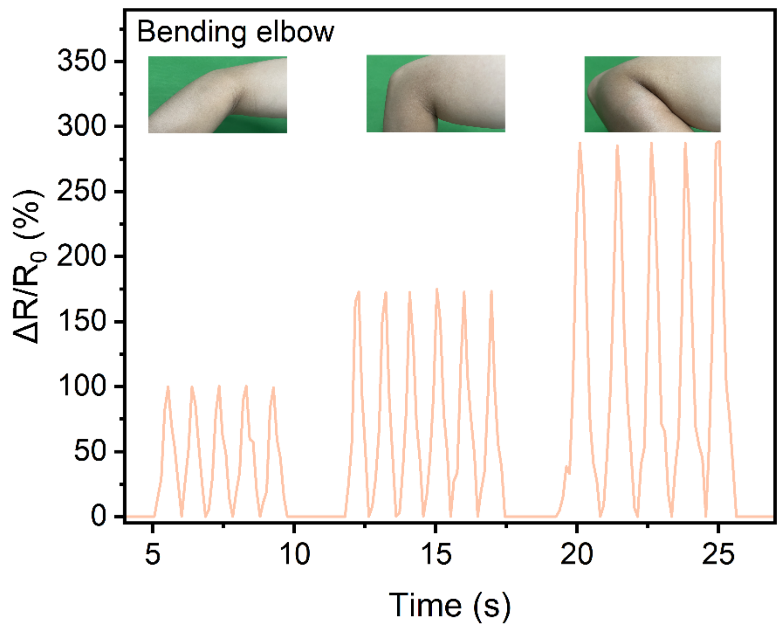

Figure S25. Continuous monitoring of elbow motions using the strain sensor at various bending angles.

7. Video

Video S1. PAA/CC adhering to finger skin and stretching deformation.

Video S2. Video of the self-healing for PAA/CC.

Video S3. After being stored at –20 °C for 24 hours, PAA/CC was subjected to a 500g weight.

Video S4. After being stored at 80 ºC for 24 hours, PAA/CC was subjected to a 500g weight.

8. References

1 Y. Liang, K. Wang, J. Li, H. Wang, X. Q. Xie, Y. Cui, Y. Zhang, M. Wang and C. Liu, *Adv. Funct.Mater.*, 2021, **31**, 2104963.

2 K. Fan, W. Wei, Z. Zhang, B. Liu, W. Feng, Y. Ma and X. Zhang, *Chem. Eng. J.*, 2022, **449**, 137878.

3 T. Chen, R. Luo, Y. Liu, L. Ma, Z. Li, C. Tao, S. Yang and J. Wang, *ACS Appl. Mater. Interfaces*, 2022, **14**, 40276–40285.

4 C. Chai, L. Ma, Y. Chu, W. Li, Y. Qian and J. Hao, *J. Colloid . Interf. Sci.*, 2023, **638**, 439–448.

5 H. Sun, B. Zhang, L. Lu, Z. Chen, Y. Huo, W. Li, B. Zhang and J. Song, *Chem. Eng. J.*, 2023, **451**, 139051.

6 Y. Wang, S. Fu, L. A. Lucia and H. Zhang, *Compos. Sci. Technol.*, 2022, **229**, 109696.

7 K. Xue, C. Shao, J. Yu, H. Zhang, B. Wang, W. Ren, Y. Cheng, Z. Jin, F. Zhang, Z. Wang and R. Sun, *Adv. Funct.Mater.*, 2023, **33**, 2305879.

8 Y. Wang, J. Wang, Z. Ma and L. Yan, *ACS Appl. Mater. Interfaces*, 2021, **13**, 54409–54416.

9 H. Zhang, N. Tang, X. Yu, M. Li and J. Hu, *Adv. Funct.Mater.*, 2022, **32**, 2206305.

10 S. Chen and J. Feng, *ACS Appl. Mater. Interfaces*, 2023, **15**, 44752–44762.

11 S. Wang, H. Cheng, B. Yao, H. He, L. Zhang, S. Yue, Z. Wang and J. Ouyang, *ACS Appl. Mater. Interfaces*, 2021, **13**, 20735–20745.

12 Y. Liang, D. Zou, Y. Zhang and Z. Zhong, *Chem. Eng. J.*, 2023, **475**, 145928.

13 X. Su, S. Zhai, K. Jin, C. Li, A. Chen, Z. Cai, C. Xian and Y. Zhao, *ACS Appl. Mater. Interfaces*, 2023, **15**, 45526–45535.

14 M. Li, Z. Liu, Y. Hu, R. a. Li and Y. Cao, *Chem. Eng. J.*, 2023, **472**, 145177.

15 J. Yang, Y. Feng, B. Wang, J. Miao, S. Wei, H. Li, L. Mo and Z. Qin, *Chem. Eng. J.*, **474**, 145544.

16 R. Zhou, Y. Jin, W. Zeng, H. Jin, L. Shi, L. Bai and X. Shang, *Adv. Funct.Mater.*, 2023, **33**, 2301921.

17 T. Lu and F. Chen, *J. Comput. Chem.*, 2012, **33**, 580–592.

18 R. M. Parrish, L. A. Burns, D. G. A. Smith, A. C. Simmonett, A. E. DePrince, 3rd, E. G. Hohenstein, U. Bozkaya, A. Y. Sokolov, R. Di Remigio, R. M. Richard, J. F. Gonthier, A. M. James, H. R. McAlexander, A. Kumar, M. Saitow, X. Wang, B. P. Pritchard, P. Verma, H. F. Schaefer, 3rd, K. Patkowski, R. A. King, E. F. Valeev, F. A. Evangelista, J. M. Turney, T. D. Crawford and C. D. Sherrill, *J. Chem. Theory Comput.*, 2017, **13**, 3185–3197.

19 T. M. Parker, L. A. Burns, R. M. Parrish, A. G. Ryno and C. D. Sherrill, *J. Chem. Phys.*, 2014, **140**, 094106.

20 Z. Long, L. You, X. Tang, W. Ma, Y. Ding and F. Xu, *Const. Build. Mater.*, 2020, **255**, 119354.

21 C. Cai, H. Gong, S. Wu, F. Li, S. Liu, Z. Tan and S. Dong, *Chem. Eng. J.*, 2023, **451**, 138674.

22 C. Cai, S. Wu, Z. Tan, F. Li and S. Dong, *ACS Appl. Mater. Interfaces*, 2021, **13**, 53083–53090.

23 Q. Lu, H. Li and Z. Tan, *ACS Appl. Mater. Interfaces*, 2023, **15**, 34055–34063.

24 K. Wang, H. Wang, J. Li, Y. Liang, X. Q. Xie, J. Liu, C. Gu, Y. Zhang, G. Zhang and C. S. Liu, *Mater. Horiz.*, 2021, **8**, 2520–2532.

25 S. Duan, Q. Shi, J. Hong, D. Zhu, Y. Lin, Y. Li, W. Lei, C. Lee and J. Wu, *ACS Nano*, 2023, **17**, 1355–1371.